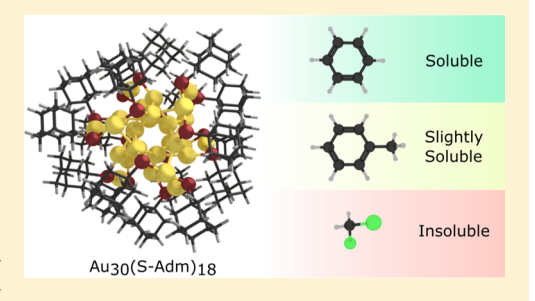
Understanding the Solubility Behavior of Atomically Precise Gold **Nanoclusters**

Michael J. Cowan,[†] Tatsuya Higaki,^{‡®} Rongchao Jin,^{‡®} and Giannis Mpourmpakis^{*,†®}

ABSTRACT: Over the last two decades, ligand-protected gold nanoclusters (Au NCs) have experienced continued interest because of their controlled synthesis with atomic precision and unique, tunable properties. Despite the success in the synthesis of a series of Au NCs, their solubility behavior as a function of size, shape, and type of ligands on their surface is not well understood. Herein, we use density functional theory calculations to systematically investigate key physicochemical properties that affect Au NC solubility in organic media. We focus on 10 experimentally determined NCs ranging from 21 to 133 Au atoms, exhibiting various shapes and stabilized by five different aprotic thiolate ligands. Our results reveal that the NC symmetry



(shape) and charge state dictate the NC dipole moment and polarizability, which in turn regulate the overall solubility behavior. Our computational results are in excellent agreement with experimental observations rationalizing solubility trends across a wide range of NC sizes. Furthermore, we demonstrate how our methodology can elucidate the atypical solubility behavior of specific Au NCs, such as Au₃₀(S-Adm)₁₈.

INTRODUCTION

Ligand-protected gold nanoclusters (Au NCs) have attracted tremendous interest owing to their atomically-precise structures and versatile functionalities.1 The exploration of intriguing properties accompanies structural determination of Au NCs, and continued progress has been made to correlate the structure with desired properties on these NCs.²⁻⁴ Recent work has demonstrated that selection of the protecting ligand can control the crystal structure of Au NCs, which in turn can dramatically enhance their functionalities, including catalytic activity, electronic excited state dynamics and photoluminescence. Further advances in synthetic chemistry is expected to devise more elegant strategies for controlling the functionality of Au NCs for applications in biomedicine, sensing, and energy storage, to name a few.

Among the physical properties of Au NCs, solubility has received little attention, yet it is critically important to many aspects of NC research. For instance, during Au NC synthesis, the choice of solvent can control the thiolate-Au speciation in solution as well as dictate the size of the final NCs.^{6,7} Moreover, in order to perform structural determination of the synthesized Au NCs, X-ray crystallography is commonly used because it is arguably the most powerful method to analyze 3D structures with atomic level precision. A prerequisite for X-ray diffraction analysis is to grow suitable single crystals of Au NCs. Crystal growth can be achieved using the vapor diffusion method where a nonsolvent is added to a concentrated solution of NCs in a solvent. 9,10 However, the pair of solvent/ nonsolvent must be properly adjusted for the specific type of surface ligands. Failure to use the appropriate solvent/

nonsolvent leads to the formation of either a powder precipitate or poorly diffractive crystals with insufficient resolution (e.g., worse than 2 Å). Thus, understanding solubility of Au NCs is essential to successful structural determination. In addition, predictive knowledge on NC solubility can aid the development of potential applications, especially in diverse environments (e.g., biological) where multicomponent phase behavior emerges.

Based on experimental observation, it is well known that the surface ligands largely determine the solubility of Au NCs, that is, organic soluble thiolate ligands (-SR) lead to $Au_n(SR)_m$ NCs soluble in common organic solvents such as toluene and dichloromethane (DCM). However, atypical solubility has been observed for some Au NCs. 10,13 For example, 1adamantanethiolate (S-Adm)-protected Au₃₀(S-Adm)₁₈ showed unexpectedly low solubility in common organic solvents and was found to only be soluble in benzene. 10 Of note, other-sized Au NCs protected by S-Adm do not exhibit this peculiar solubility, 14,15 revealing that there must be factors besides ligand type contributing to the overall solubility behavior. The unique insolubility of Au₃₀(S-Adm)₁₈ in common organic solvents indeed allowed for an efficient removal of impurities to accordingly obtain the molecularly pure main product. Furthermore, dissolving Au₃₀(S-Adm)₁₈ in benzene and using a suitable nonsolvent allowed for successful crystallization of the Au NC.10

Received: June 11, 2019 Revised: July 17, 2019 Published: July 22, 2019

Department of Chemical Engineering, University of Pittsburgh, Pittsburgh, Pennsylvania 15261, United States Department of Chemistry, Carnegie Mellon University, Pittsburgh, Pennsylvania 15213, United States

Supporting Information

Although leveraging the unique solubility behavior of Au₃₀(S-Adm)₁₈ enabled its effective synthesis and crystal growth, it is still not well understood why the NC exhibits these properties. In fact, very little work has been performed on the understanding of solvent-NC interactions for any metal NCs. 16,17 As for other material classes, electronic properties, which dictate intermolecular interactions, have been shown to play a significant role in solubility behavior. ¹⁸ For example, in a recent computational study, it was found that the polarity (i.e., permanent dipole moment) of C60 fullerene derivatives directly affected their solubility in water. 19 Other works have revealed that molecular polarizability, both of the solute and solvent, is a major factor that dictates solubility of organic systems. 20-24 Inspired by these studies and considering Au NCs as inorganic-organic hybrid molecules,²⁵ we focus on experimentally determined Au NCs of different morphologies 9,10,14,15,26-31 and determine electronic properties (e.g., dipole moment and molecular polarizability) that are critical to modulating solubility behavior using first-principles calculations. Combining our computational results with experimental observations, we set rules for rationalizing NC solubility trends in organic media.

COMPUTATIONAL DETAILS

All calculations were implemented with the CP2K package.³² Density functional theory (DFT) calculations were performed using the Perdew-Burke-Ernzerhof (PBE)³³ exchangecorrelation functional with a 500 Ry energy cutoff, double- ζ polarized basis set, 32,34 and Goedecker-Teter-Hutter 33 pseudopotentials. PBE was selected due to its proven success in calculating electronic properties of Au NCs. 3,15,27 All NCs were centered in a nonperiodic cubic box with a 7 Å minimum offset between the structure and boundary. The systems were then relaxed until interatomic forces were no greater than 2 × 10⁻² eV/Å. Self-consistent field energies were converged to 10⁻⁷ Ha. The fully optimized structures were then used to calculate the electronic permanent dipole vectors and polarizability tensors of the Au NCs. Total electronic dipole moments were calculated based on the generation of maximally localized Wannier functions using the Berry phase scheme. 36-38 The dipole moment vectors (see Table S1) were found relative to the center-of-mass of each Au NC. Magnitudes of the dipole vectors (μ) were calculated by

$$\mu = \sqrt{\mu_x^2 + \mu_y^2 + \mu_z^2} \tag{1}$$

where μ_i is the *i*th (x, y, z) component of the dipole vector. Electronic polarizability tensor calculations were performed with the variational perturbation theory using a diagonalization-based preconditioned conjugate gradient approach.³⁹ The optimized NCs were placed in a polar environment, and the response wave functions were converged in a self-consistent manner to 10⁻⁶ Ha. The resulting tensors were diagonalized to find the molecular polarizabilities of each Au NC (see Table S2).⁴⁰ The average polarizability (α) and anisotropy ($\Delta \alpha$) were calculated as

$$\alpha = \frac{(\alpha_{xx} + \alpha_{yy} + \alpha_{zz})}{3} \tag{2}$$

$$\Delta \alpha = \frac{1}{\sqrt{2}} \sqrt{(\alpha_{xx} - \alpha_{yy})^2 + (\alpha_{yy} - \alpha_{zz})^2 + (\alpha_{zz} - \alpha_{xx})^2}$$

where α_{ii} corresponds to the principal components (i.e., diagonal terms) of the molecular polarizability. 40,41

RESULTS AND DISCUSSION

We first list the experimental observations of solubility for 10 Au NCs in Table 1. The results reveal the common solubility

Table 1. Experimental Solubility Behavior of Ten Au NCs [Including Neutral and Anionic Forms of Au₂₅(PET)₁₈]^a

name	solvent	nonsolvent	ref(s)
Au ₂₁ (S-Adm) ₁₅	Tol, DCM	MeOH, ACN	15
$\mathrm{Au}_{25}(\mathrm{PET})_{18}$	Ben, Tol, DCM	EtOH, ACN	13, 31, and 43
$[Au_{25}(PET)_{18}]^{-}[TOA]^{+}$	Ben, Tol, DCM, ACN	EtOH	13, 43, and 44
$\mathrm{Au}_{28}(\mathrm{TBBT})_{20}$	Tol, DCM	MeOH, EtOH	28 and 45
Au ₃₀ (S-Adm) ₁₈	Ben	Tol ^b , Chloroform ^b , DCM, THF, MeOH, ACN, acetone	10
$Au_{30}S(S-{}^tBut)_{18}$	Tol, DCM, THF	MeOH, EtOH	27 and 46
$Au_{36}(TBBT)_{24}$	Tol, DCM	EtOH	29 and 45
$Au_{38}S_2(S-Adm)_{20}$	Tol, DCM	MeOH	14
$\mathrm{Au}_{40}(o\text{-MBT})_{24}$	Tol, DCM	MeOH	26 and 47
$Au_{52}(TBBT)_{32}$	Tol, DCM	MeOH	26 and 45
$Au_{133}(TBBT)_{52}$	Tol, DCM, THF	MeOH, EtOH, ACN	9 and 48

^aBen: benzene, Tol: toluene, DCM: dichloromethane, MeOH: methanol, EtOH: ethanol, ACN: acetonitrile, THF: tetrahydrofuran. Described as "slightly soluble".

properties of Au NCs protected by aprotic thiolate ligands. Specifically, this class of Au NCs is typically soluble in toluene and DCM but insoluble in protic solvents such as methanol and ethanol. These Au NCs are also generally insoluble in aprotic solvents with a relatively large dipole moment such as acetonitrile. Of particular note within Table 1 are the anionic Au₂₅(PET)₁₈ stabilized with a tetraoctylammonium (TOA⁺) counterion and Au₃₀(S-Adm)₁₈. These two systems do not follow the aforementioned standard solubility properties. For $[Au_{25}(PET)_{18}]^{-}[TOA]^{+}$, we note that its neutral counterpart exhibits typical solubility, indicating the importance of the total charge state to solubility behavior. As previously stated, the Au₃₀(S-Adm)₁₈ NC is only soluble in nonpolar benzene, which is drastically different than the other two Au NCs protected by the same ligand [i.e., $Au_{38}S_2(S-Adm)_{20}$ and $Au_{21}(S-Adm)_{15}$]. We examine this atypical solubility behavior by first utilizing Hansen solubility parameters (HSPs), a similarity metric used to determine solubility between organic molecules.⁴² In Figure S1, we plot HSPs of the solvents tested for $Au_{30}(S-Adm)_{18}$. By coloring the points based on solubility behavior of the NC, one can immediately notice the distinct regions that appear in the HSP space. Taking the HSP of benzene as the reference point, we observe that as one traverses further away in the HSP space, the solubility behavior shifts to "slightly soluble" and then to insoluble. Although the results agree with experimental observations, they do not rationalize the unusual solubility behavior of Au₃₀(S-Adm)₁₈ when compared to other Au NCs. Instead, a more thorough analysis of all Au NCs presented in Table 1 is required that focuses on their inherent properties.

The Journal of Physical Chemistry C

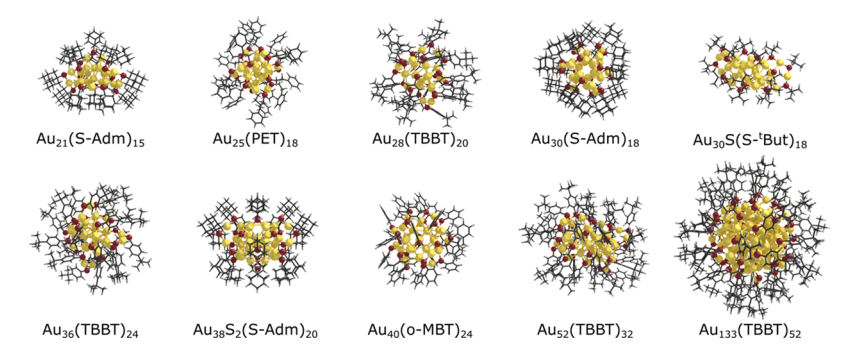


Figure 1. Ligand-protected Au NCs fully optimized with DFT. Gold and red balls correspond to Au and S atoms, respectively. Black and white sticks represent hydrocarbon ligands. S-Adm: 1-adamantanethiolate, PET: 2-phenylethanethiolate, TBBT: 4-tert-butylbenzenethiolate, S-^tBut: tert-butylthiolate, o-MBT: ortho-methylbenzenethiolate.

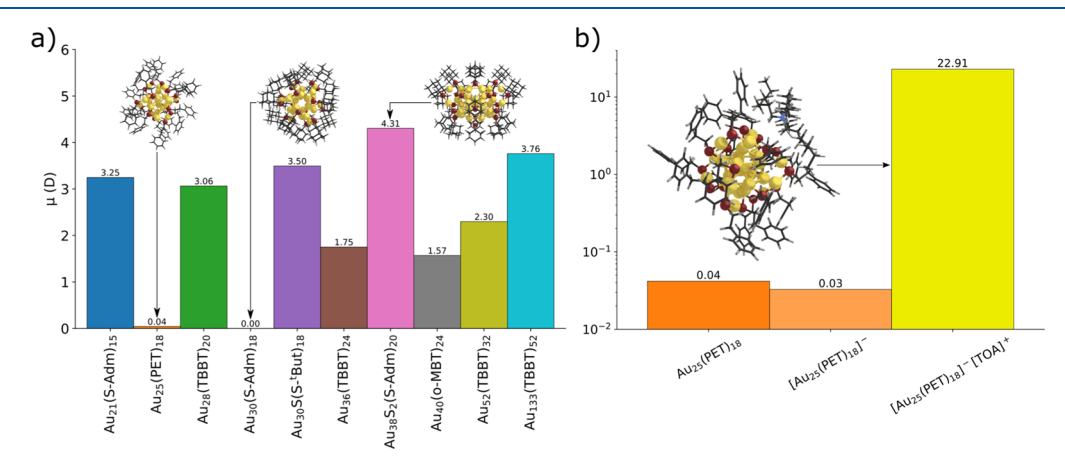


Figure 2. Magnitude of total electronic dipole moment vectors (in Debye) for (a) 10 neutral NCs (in the order of increasing number of Au) and (b) $Au_{25}(PET)_{18}$ in the neutral and anionic charge states and in the presence of a TOA^+ (tetraoctylammonium) counterion (inset structure). The structures exhibiting the minimum $[Au_{25}(PET)_{18}$ and $Au_{30}(S-Adm)_{18}]$ and maximum $(Au_{38}S_2(S-Adm)_{20})$ permanent dipoles are shown as insets in the left panel.

To understand the solubility properties of the Au NCs listed in Table 1, we first optimized their experimentally determined structures using DFT. The ten (neutral) systems shown in Figure 1 represent a wide range of Au NCs varying in size (21-133 Au atoms), ligand type (five different organic ligands), and shape (i.e., symmetry). Although diverse, these structures generally follow the divide-and-protect theory of Au NCs. 49 In short, the NCs exhibit a symmetric Au core protected by a shell of RS-(Au-SR)_n "staple" motifs. Additionally, the Au NCs follow a universal nanoscaling law in which Au and ligand counts are representative of NC volume and surface area, respectively.^{3,4,50} Because of this relationship, the ligand coverage for all Au NCs surrounds their respective Au core with a rough uniform density. Besides the neutral NCs, we also optimized the anionic [Au₂₅(PET)₁₈] NC with and without the presence of TOA⁺. The structure of the relaxed $[Au_{25}(PET)_{18}]^-[TOA^+]$ is presented in Figure 2b. For a complete list of NC point group symmetry and optimized atomic coordinates, see Tables S3 and S4, respectively.

Studying Au NCs with similar structural properties but different solubility behaviors enables us to systematically examine the role that specific physicochemical properties play in solubility. For example, from Table 1, one can observe that Au NCs protected by TBBT are found to have typical solubility, independent of size. However, this trend breaks down when one looks at (S-Adm)-protected NCs. In fact,

there appears to be no correlation between solubility and NC size, suggesting that the solubility behavior of Au NCs is sizeagnostic. Focusing on Au NC shape instead leads to some interesting comparisons between structures. For instance, the atypical solubility behavior of Au₃₀(S-Adm)₁₈ could be attributed to its relatively high symmetry (i.e., S₆ point group). 10 The only NC with a higher order of symmetry is the $Au_{25}(PET)_{18}$ (D_{2h} point group). However, the anionic form of the Au₂₅(PET)₁₈ is stabilized by the presence of a TOA⁺ counterion. Because of the equal concentrations of $[\mathrm{Au}_{25}(\mathrm{PET})_{18}]^-$ and TOA^+ in solution, the counterion must be considered when examining NC symmetry. Thus, the presence of TOA^+ breaks the D_{2h} symmetry of the system. Furthermore, the loss of an electron to form the neutral Au₂₅(PET)₁₈ results in a slight distortion of the NC. This distortion arises from the open-shell 1S21P5 superatom electron configuration.⁵¹ Therefore, our qualitative observations suggest that symmetry plays a key role in Au NC solubility behavior.

Permanent dipole moment of solutes can affect their solubility behavior. Additionally, dipole moment serves as a means to address symmetry effects in charge distribution on a chemical structure. Therefore, we calculated the total electronic dipole moment of each Au NC (Figure 2) to quantitatively analyze these effects—connecting NC symmetry to solubility behavior. Of the 10 neutral Au NCs studied (shown in Figure 2a), Au₃₈S₂(S-Adm)₁₈ exhibits the largest

dipole moment of 4.31 D. This can be attributed to the two μ_3 sulfido atoms located on a single side of the NC, leading to $C_{2\nu}$ symmetry. 14 The presence of nonsymmetrically (i.e., lacking a horizontal mirror plane) distributed sulfido atoms strongly influences the dipole moment as also indicated by Au₃₀S-(S-^tBut)₁₈, which has a large dipole of 3.50 D. However, in the absence of sulfido atoms, NC symmetry appears to play the major role. In fact, the orientation of the protecting thiolate ligands can have a significant impact on the resulting electronic dipole of Au NCs. This becomes apparent in the largest NC that we investigated. Au₁₃₃(TBBT)₅₂ has a highly symmetric Mackay icosahedral Au core, but its "swirly" distribution of surface ligands breaks the total symmetry of the system.⁴⁸ Thus, we find the Au₁₃₃ NC to exhibit the second largest dipole moment of 3.76 D. Although the anionic state of the Au₂₅(PET)₁₈ NC has been reported to have higher symmetry than the neutral, 51,52 the presence of the TOA+ counterion must be considered when calculating its dipole moment calculation. As previously stated, this is due to $[Au_{25}(PET)_{18}]^{-}$ and TOA+ having equivalent concentrations in solution. Thus, there are 1:1 electronic interactions exhibited between the NCs and counterions which must be accounted for. Although the counterion and the anionic NC are expected to be solvated in solution, decreasing their intermolecular interactions (compared to gas phase), a dipole is expected to be developed because a negative charge is equilibrated in the vicinity of a positive charge in solution. As a result, including TOA⁺ in our calculation generates a strong electronic dipole of 22.91 Debye (Figure 2b). We note that strong interactions also exist due to the NC charge and the dipole of the solvent. However, for the purposes of gaining trends with a single NC descriptor, we can capture these charge effects through our electronic dipole moment calculations, where the dipole moment becomes significant between two point charges (charged NC and counterion). The drastic increase in the dipole moment explains why $[Au_{25}(PET)_{18}]^{-}[TOA]^{+}$ has the unique ability to dissolve in the highly polar acetonitrile. Additionally, the result reveals the importance that the charge state of Au NCs has on their solubility properties. This is especially significant for larger Au NCs because determining the correct charge for some of these systems has been shown to be a difficult task.53,54

As previously mentioned, $Au_{30}(S-Adm)_{18}$ exhibits the second highest order symmetry of the NCs studied herein. As a further indication of high symmetry, the Au₃₀(S-Adm)₁₈ NC was found to be perfectly nonpolar with a calculated dipole moment of 0.00 D. The lack of dipole can easily be realized through visualizing the electron density and charge distribution within the Au NC. Figure S2 reveals symmetric charge density that can be seen through a continuum of charge isosurfaces (Figure S2a) as well as atomic point charges (Figure S2b). The result is in striking contrast to the polar Au₂₁(S-Adm)₁₅ and $Au_{38}S_2(S-Adm)_{20}$ NCs that are stabilized with the same type of ligands. Moreover, the results for (S-Adm)-protected NCs strongly agree with the experimental observations, suggesting that the presence of an electronic dipole moment is essential for a NC to exhibit typical solubility behavior (i.e., NC soluble in toluene and DCM). However, the neutral Au₂₅(PET)₁₈ also exhibits no dipole with a calculated value of 0.04 D, yet it follows typical NC solubility. Therefore, although important, the permanent dipole moment alone does not completely explain Au NC solubility behavior.

Because polarizability has been shown to be a key factor in solubility behavior of molecular systems, 20-24 we calculated the molecular electronic polarizability of the 10 Au NCs. As expected based on previous work with organic molecules, 41 we found a strong linear correlation between the average polarizability and the size of each system (using the number of electrons in each system as a descriptor), as shown in Figure S3. Furthermore, Figure S3 reveals that for Au NCs with the same ligand type (S-Adm and TBBT), we find perfect linear relationships but with different slopes. The slight difference in slope can be attributed to the difference in saturation of hydrocarbons between ligand types. 41 In an effort to further understand the polarizability behavior of the NCs we examine the anisotropy of the polarizability as shown in Figure 3. One

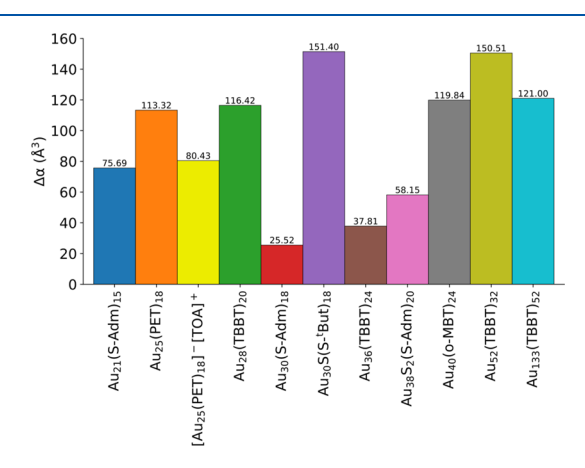


Figure 3. Polarizability anisotropy $(\Delta \alpha)$ of Au NCs in the order of increasing number of Au atoms. Anisotropy is given in units of Å³.

can immediately notice the unique character of the nonpolar Au₃₀(S-Adm)₁₈ NC as it is found to exhibit the lowest anisotropy at 25.52 Å³. This is in stark contrast to the other nonpolar NC studied, the neutral Au₂₅(PET)₁₈, as it has an anisotropy that is over three times greater (80.43 Å³). This difference in the polarizability anisotropy can rationalize the unique behavior of the two NCs, Au₃₀(S-Adm)₁₈ and Au₂₅(PET)₁₈. Specifically, to relate these results to solubility, we first note our assumption that in solution, each of the two Au NCs experiences a uniform and symmetric solvation environment. This is a legitimate assumption accounting for the fact that each Au NC is protected by a single ligand type, and the ligand coverage is generally uniform across the NC surface (supported by the aforementioned nanoscaling law, where the number of surface ligands scales with the number of Au atoms on $\operatorname{Au}_n(\operatorname{SR})_m$ NCs, as $m \propto n^{2/3}$. As a result, a larger anisotropy in polarizability would lead to a stronger induced dipole within a Au NC. This is due to the electronic structure of a NC becoming polarized through intermolecular interactions with the solvent in an increasing manner for systems that exhibit higher anisotropy in polarizability. Thus, because Au₃₀(S-Adm)₁₈ is closer to isotropic polarizability, it experiences a smaller induced dipole in solution, which suggests its inability to dissolve in solvents with a permanent dipole moment, such as DCM and toluene. In contrast, the larger anisotropy of the neutral Au₂₅(PET)₁₈ would experience a greater induced dipole, leading to its solubility in toluene and

To further rationalize Au NC solubility trends with our electronic property calculations, we plot dipole moment, anisotropy, and experimental solubility behavior in Figure 4. The plot demonstrates the clear distinctions that differentiate

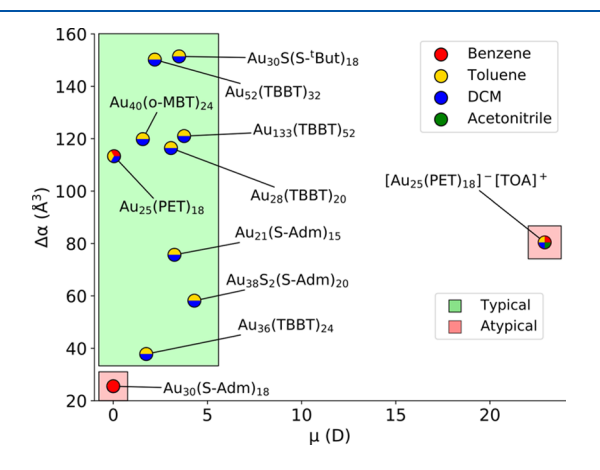


Figure 4. Comparing permanent dipole moment and anisotropy to Au NC solubility behavior. Data point colors indicate observed solvents for each Au NC. Boxes represent regions of typical (green) and atypical (red) solubility behavior.

 $Au_{30}(S-Adm)_{18}$ and $[Au_{25}(PET)_{18}]^{-}[TOA]^{+}$ from NCs with typical solubility. In fact, by defining regions on Figure 4 that correspond to different solubility behaviors, we reveal an excellent agreement between our computational results and the experimental observations. Moreover, our findings suggest that dipole moment and anisotropy can be used in concert as parameters to predict the solubility behavior of all Au NCs protected by aprotic, thiolate ligands. The approach can also be applied to other metal NCs protected by the same ligand type. For instance, [Ag₂₅(SR)₁₈]⁻[PPh₄]⁺, protected by 2-4dimethylbenzenethiolate, has been successfully synthesized and was found to be an analogue to anionic Au₂₅(PET)₁₈ (i.e., same shape and symmetry).⁵⁸ It also shares similar solubility behavior to its Au counterpart. Specifically, the Ag NC is soluble in aprotic solvents (DCM, dimethylformamide, dimethyl sulfoxide, and toluene) and insoluble in methanol. Additionally, the Ag NC is soluble in a 1:1 v/v solution of DCM and acetonitrile, supporting the role that the charge state plays in solubility behavior. Our methods can also be extended to heterometal-doped NCs,⁵⁶ a field that is quickly growing due to the potential bimetallic NCs have for use in applications such as catalysis.⁵⁷ To test the effect of heterometal doping, we created a theoretical Au₂₉Ag(S-Adm)₁₈ NC and calculated its dipole moment and anisotropy. As shown in Figure S4, doping a Ag atom in the shell of the NC breaks its symmetry, thus creating a permanent dipole moment (from 0.00 to 0.852 D). However, there is almost no change in the anisotropy of the system. The results suggest that heterometal doping could provide a means of control over the solubility behavior of metal NCs.

Although our work agrees well with the experiment, we note that further investigations studying the explicit, dynamic interactions between metal NCs and solvents are needed to completely understand NC solubility behavior. Nevertheless, the picture that emerges from static DFT calculations is powerful and rapid (compared to time-demanding first-principles molecular dynamics simulations) in rationalizing solubility trends based solely on electronic properties of NCs.

CONCLUSIONS

In summary, we used DFT calculations to investigate the solubility properties of 10 Au NCs. Our results show the essential roles that permanent dipole moment and polarizability play in determining which solvents can dissolve a given Au NC. For neutral Au NCs with typical solubility (soluble in toluene and DCM), we found that the structures generally exhibit a dipole moment of 1.5-4.5 D and anisotropy above 35 Å³. The anionic Au₂₅(PET)₁₈ was found to have a high dipole moment due to the presence of the TOA+ counterion. The large dipole moment explains why the NC can dissolve in the polar acetonitrile as well as the typical Au NC solvents. The result demonstrates the importance of the charge state and the presence of counterions when determining the solubility properties of Au NCs. Au₃₀(S-Adm)₁₈—a second NC with atypical solubility—was found to be nonpolar and additionally has extremely low anisotropy, which leads to its inability to dissolve in polar organic solvents. Neutral $Au_{25}(PET)_{18}$ was also found to be nonpolar, but it exhibits high anisotropy. This suggests that a dipole can be induced in the Au NC, enabling it to dissolve in the common Au NC solvents, that is, toluene and DCM. Importantly, our calculations rationalize a series of experimental observations with regards to the solubility behavior of Au NCs that exhibit diverse structures (i.e., size, shape, and ligands) and offer rapid and powerful means to address solubility trends within different NCs, by calculating their electronic properties such as dipole moment and polarizability.

ASSOCIATED CONTENT

S Supporting Information

The Supporting Information is available free of charge on the ACS Publications website at DOI: 10.1021/acs.jpcc.9b05562.

Au NC dipole moment and polarizability raw data, $\mathrm{Au}_{30}(\mathrm{S-Adm})_{18}$ solubility behavior compared to HSPs, charge density maps of $\mathrm{Au}_{30}(\mathrm{S-Adm})_{18}$, average polarizability plotted against number of electrons in each Au NC, structure and electronic properties of theoretical $\mathrm{Au}_{29}\mathrm{Ag}(\mathrm{S-Adm})_{18}$, point group symmetry of Au NCs calculated by excluding R group in ligands, and optimized atomic coordinates of Au NCs (PDF)

AUTHOR INFORMATION

Corresponding Author

*E-mail: gmpourmp@pitt.edu.

ORCID 6

Tatsuya Higaki: 0000-0002-6759-9009 Rongchao Jin: 0000-0002-2525-8345

Giannis Mpourmpakis: 0000-0002-3063-0607

Notes

The authors declare no competing financial interest.

ACKNOWLEDGMENTS

The work herein was supported by the National Science Foundation (NSF, CBET-CAREER program) under grant no. 1652694. The authors would like to acknowledge computational support from the Center for Research Computing (CRC) at the University of Pittsburgh and the Extreme Science and Engineering Discovery Environment (XSEDE), which is supported by the NSF (ACI-1548562). R.J. acknowledges financial support from the National Science

Foundation (DMR-1808675) and the Air Force Office of Scientific Research.

REFERENCES

- (1) Jin, R.; Zeng, C.; Zhou, M.; Chen, Y. Atomically Precise Colloidal Metal Nanoclusters and Nanoparticles: Fundamentals and Opportunities. *Chem. Rev.* **2016**, *116*, 10346–10413.
- (2) Du, Y.; Sheng, H.; Astruc, D.; Zhu, M. Atomically Precise Noble Metal Nanoclusters as Efficient Catalysts: A Bridge between Structure and Properties. *Chem. Rev.* **2019**, DOI: 10.1021/acs.chemrev.8b00726.
- (3) Cowan, M. J.; Mpourmpakis, G. Structure-property relationships on thiolate-protected gold nanoclusters. *Nanoscale Adv.* **2019**, *1*, 184–188.
- (4) Taylor, M. G.; Mpourmpakis, G. Thermodynamic stability of ligand-protected metal nanoclusters. *Nat. Commun.* **2017**, *8*, 15988.
- (5) Higaki, T.; Li, Q.; Zhou, M.; Zhao, S.; Li, Y.; Li, S.; Jin, R. Toward the Tailoring Chemistry of Metal Nanoclusters for Enhancing Functionalities. *Acc. Chem. Res.* **2018**, *51*, 2764–2773.
- (6) Mpourmpakis, G.; Caratzoulas, S.; Vlachos, D. G. What Controls Au Nanoparticle Dispersity during Growth? *Nano Lett.* **2010**, *10*, 3408–3413.
- (7) Jiang, Y.; Huang, Y.; Cheng, H.; Liu, Q.; Xie, Z.; Yao, T.; Jiang, Z.; Huang, Y.; Bian, Q.; Pan, G.; et al. Solvent Influence on the Role of Thiols in Growth of Thiols-Capped Au Nanocrystals. *J. Phys. Chem.* C **2014**, *118*, 714–719.
- (8) Billinge, S. J. L.; Levin, I. The Problem with Determining Atomic Structure at the Nanoscale. *Science* **2007**, *316*, 561.
- (9) Dass, A.; Theivendran, S.; Nimmala, P. R.; Kumara, C.; Jupally, V. R.; Fortunelli, A.; Sementa, L.; Barcaro, G.; Zuo, X.; Noll, B. C. Au₁₃₃(SPh-tBu)₅₂ Nanomolecules: X-ray Crystallography, Optical, Electrochemical, and Theoretical Analysis. *J. Am. Chem. Soc.* **2015**, 137, 4610–4613.
- (10) Higaki, T.; Liu, C.; Zeng, C.; Jin, R.; Chen, Y.; Rosi, N. L.; Jin, R. Controlling the Atomic Structure of Au₃₀ Nanoclusters by a Ligand-Based Strategy. *Angew. Chem., Int. Ed.* **2016**, 55, 6694–6697.
- (11) Yan, N.; Xia, N.; Liao, L.; Zhu, M.; Jin, F.; Jin, R.; Wu, Z. Unraveling the long-pursued Au₁₄₄ structure by x-ray crystallography. *Sci. Adv.* **2018**, *4*, No. eaat7259.
- (12) Koivisto, J.; Salorinne, K.; Mustalahti, S.; Lahtinen, T.; Malola, S.; Häkkinen, H.; Pettersson, M. Vibrational Perturbations and Ligand–Layer Coupling in a Single Crystal of $Au_{144}(SC_2H_4Ph)_{60}$ Nanocluster. J. Phys. Chem. Lett. **2014**, 5, 387–392.
- (13) Qian, H.; Sfeir, M. Y.; Jin, R. Ultrafast Relaxation Dynamics of $[Au_{25}(SR)_{18}]^q$ Nanoclusters: Effects of Charge State. *J. Phys. Chem. C* **2010**, *114*, 19935–19940.
- (14) Liu, C.; Li, T.; Li, G.; Nobusada, K.; Zeng, C.; Pang, G.; Rosi, N. L.; Jin, R. Observation of Body-Centered Cubic Gold Nanocluster. *Angew. Chem.* **2015**, *54*, 9826–9829.
- (15) Chen, S.; Xiong, L.; Wang, S.; Ma, Z.; Jin, S.; Sheng, H.; Pei, Y.; Zhu, M. Total Structure Determination of Au₂₁(S-Adm)₁₅ and Geometrical/Electronic Structure Evolution of Thiolated Gold Nanoclusters. *J. Am. Chem. Soc.* **2016**, *138*, 10754–10757.
- (16) Zhou, M.; Lei, Z.; Guo, Q.; Wang, Q.-M.; Xia, A. Solvent Dependent Excited State Behaviors of Luminescent Gold(I)-Silver(I) Cluster with Hypercoordinated Carbon. *J. Phys. Chem. C* **2015**, *119*, 14980–14988.
- (17) Pei, X.-L.; Yang, Y.; Lei, Z.; Wang, Q.-M. Geminal Tetraauration of Acetonitrile: Hemilabile-Phosphine-Stabilized Au₈Ag₄ Cluster Compounds. *J. Am. Chem. Soc.* **2013**, *135*, 6435–6437.
- (18) Chernyak, Y. Dielectric Constant, Dipole Moment, and Solubility Parameters of Some Cyclic Acid Esters. *J. Chem. Eng. Data* **2006**, *51*, 416–418.
- (19) Zhu, J.; Ou, X.; Su, J.; Li, J. The impacts of surface polarity on the solubility of nanoparticle. *J. Chem. Phys.* **2016**, *145*, 044504.
- (20) Kamlet, M. J.; Doherty, R. M.; Taft, R. W.; Abraham, M. H.; Koros, W. J. Solubility properties in polymers and biological mediums. 3. Predictional methods for critical temperatures, boiling points, and

- solubility properties (RG values) based on molecular size, polarizability, and dipolarity. *J. Am. Chem. Soc.* **1984**, *106*, 1205–1212.
- (21) Dyer, P. J.; Docherty, H.; Cummings, P. T. The importance of polarizability in the modeling of solubility: Quantifying the effect of solute polarizability on the solubility of small nonpolar solutes in popular models of water. *J. Chem. Phys.* **2008**, *129*, 024508.
- (22) Campanell, F. C.; Battino, R.; Seybold, P. G. On the Role of Solute Polarizability in Determining the Solubilities of Gases in Liquids. *J. Chem. Eng. Data* **2010**, *55*, 37–40.
- (23) Herbst, M. H.; Dias, G. H. M.; Magalhães, J. G.; Tôrres, R. B.; Volpe, P. L. O. Enthalpy of solution of fullerene[60] in some aromatic solvents. *J. Mol. Liq.* **2005**, *118*, 9–13.
- (24) Chenzhong, C.; Zhiliang, L. Molecular Polarizability. 1. Relationship to Water Solubility of Alkanes and Alcohols. *J. Chem. Inf. Comput. Sci.* **1998**, 38, 1–7.
- (25) Jin, R. Atomically precise metal nanoclusters: stable sizes and optical properties. *Nanoscale* **2015**, *7*, 1549–1565.
- (26) Zeng, C.; Chen, Y.; Liu, C.; Nobusada, K.; Rosi, N. L.; Jin, R. Gold tetrahedra coil up: Kekulé-like and double helical super-structures. *Sci. Adv.* **2015**, *1*, No. e1500425.
- (27) Crasto, D.; Malola, S.; Brosofsky, G.; Dass, A.; Häkkinen, H. Single Crystal XRD Structure and Theoretical Analysis of the Chiral Au₃₀S(S-t-Bu)₁₈ Cluster. *J. Am. Chem. Soc.* **2014**, *136*, 5000–5005.
- (28) Zeng, C.; Li, T.; Das, A.; Rosi, N. L.; Jin, R. Chiral Structure of Thiolate-Protected 28-Gold-Atom Nanocluster Determined by X-ray Crystallography. *J. Am. Chem. Soc.* **2013**, *135*, 10011–10013.
- (29) Zeng, C.; Qian, H.; Li, T.; Li, G.; Rosi, N. L.; Yoon, B.; Barnett, R. N.; Whetten, R. L.; Landman, U.; Jin, R. Total Structure and Electronic Properties of the Gold Nanocrystal Au₃₆(SR)₂₄. Angew. Chem. **2012**, *S1*, 13114–13118.
- (30) Heaven, M. W.; Dass, A.; White, P. S.; Holt, K. M.; Murray, R. W. Crystal Structure of the Gold Nanoparticle $[N(C_8H_{17})_4]$ - $[Au_{25}(SCH_2CH_2Ph)_{18}]$. J. Am. Chem. Soc. **2008**, 130, 3754–3755.
- (31) Zhu, M.; Eckenhoff, W. T.; Pintauer, T.; Jin, R. Conversion of Anionic [Au₂₅(SCH₂CH₂Ph)₁₈]—Cluster to Charge Neutral Cluster via Air Oxidation. *J. Phys. Chem. C* **2008**, *112*, 14221–14224.
- (32) Hutter, J.; Iannuzzi, M.; Schiffmann, F.; VandeVondele, J. cp2k: atomistic simulations of condensed matter systems. *Wiley Interdiscip. Rev.: Comput. Mol. Sci.* **2013**, *4*, 15–25.
- (33) Perdew, J. P.; Burke, K.; Ernzerhof, M. Generalized Gradient Approximation Made Simple. *Phys. Rev. Lett.* **1996**, *77*, 3865–3868.
- (34) VandeVondele, J.; Hutter, J. Gaussian basis sets for accurate calculations on molecular systems in gas and condensed phases. *J. Chem. Phys.* **2007**, *127*, 114105.
- (35) Goedecker, S.; Teter, M.; Hutter, J. Separable dual-space Gaussian pseudopotentials. *Phys. Rev. B* **1996**, *54*, 1703–1710.
- (36) Silvestrelli, P. L.; Parrinello, M. Structural, electronic, and bonding properties of liquid water from first principles. *J. Chem. Phys.* **1999**, *111*, 3572–3580.
- (37) Marzari, N.; Vanderbilt, D. Maximally localized generalized Wannier functions for composite energy bands. *Phys. Rev. B* **1997**, *56*, 12847–12865.
- (38) Berry, M. V. Quantal phase factors accompanying adiabatic changes. *Proc. R. Soc. London, Ser. A* **1984**, 392, 45–57.
- (39) Putrino, A.; Sebastiani, D.; Parrinello, M. Generalized variational density functional perturbation theory. *J. Chem. Phys.* **2000**, *113*, 7102–7109.
- (40) Miller, K. J. Calculation of the molecular polarizability tensor. *J. Am. Chem. Soc.* **1990**, *112*, 8543–8551.
- (41) Gussoni, M.; Rui, M.; Zerbi, G. Electronic and relaxation contribution to linear molecular polarizability. An analysis of the experimental values. *J. Mol. Struct.* **1998**, 447, 163–215.
- (42) Hansen, C. M. Hansen Solubility Parameters: A User's Handbook, 2 ed.; CRC Press, 2007.
- (43) Pengo, P.; Bazzo, C.; Boccalon, M.; Pasquato, L. Differential reactivity of the inner and outer positions of $Au_{25}(SCH_2CH_2Ph)_{18}$ dimeric staples under place exchange conditions. *Chem. Commun.* **2015**, *51*, 3204–3207.

- (44) Zhu, M.; Aikens, C. M.; Hollander, F. J.; Schatz, G. C.; Jin, R. Correlating the crystal structure of a thiol-protected Au₂₅ cluster and optical properties. *J. Am. Chem. Soc.* **2008**, *130*, 5883–5885.
- (45) Zhou, M.; Zeng, C.; Sfeir, M. Y.; Cotlet, M.; Iida, K.; Nobusada, K.; Jin, R. Evolution of Excited-State Dynamics in Periodic Au₂₈, Au₃₆, Au₄₄, and Au₅₂ Nanoclusters. *J. Phys. Chem. Lett.* **2017**, 8, 4023–4030.
- (46) Yang, H.; Wang, Y.; Edwards, A. J.; Yan, J.; Zheng, N. High-yield synthesis and crystal structure of a green Au₃₀ cluster co-capped by thiolate and sulfide. *Chem. Commun.* **2014**, *50*, 14325–14327.
- (47) Chen, Y.; Zeng, C.; Kauffman, D. R.; Jin, R. Tuning the Magic Size of Atomically Precise Gold Nanoclusters via Isomeric Methylbenzenethiols. *Nano Lett.* **2015**, *15*, 3603–3609.
- (48) Zeng, C.; Chen, Y.; Kirschbaum, K.; Appavoo, K.; Sfeir, M. Y.; Jin, R. Structural patterns at all scales in a nonmetallic chiral Au₁₃₃(SR)₅₂ nanoparticle. *Sci. Adv.* **2015**, *1*, No. e1500045.
- (49) Häkkinen, H.; Walter, M.; Grönbeck, H. Divide and Protect: Capping Gold Nanoclusters with Molecular Gold—Thiolate Rings. *J. Phys. Chem. B* **2006**, *110*, 9927—9931.
- (50) Dass, A. Nano-scaling law: geometric foundation of thiolated gold nanomolecules. *Nanoscale* **2012**, *4*, 2260–2263.
- (51) Tofanelli, M. A.; Salorinne, K.; Ni, T. W.; Malola, S.; Newell, B.; Phillips, B.; Häkkinen, H.; Ackerson, C. J. Jahn-Teller effects in Au₂₅(SR)₁₈. *Chem. Sci.* **2016**, *7*, 1882–1890.
- (\$2) Kang, X.; Chong, H.; Zhu, M. Au₂₅(SR)₁₈: the captain of the great nanocluster ship. *Nanoscale* **2018**, *10*, 10758–10834.
- (53) Vergara, S.; Lukes, D. A.; Martynowycz, M. W.; Santiago, U.; Plascencia-Villa, G.; Weiss, S. C.; de la Cruz, M. J.; Black, D. M.; Alvarez, M. M.; López-Lozano, X.; et al. MicroED Structure of Au₁₄₆(p-MBA)₅₇ at Subatomic Resolution Reveals a Twinned FCC Cluster. *J. Phys. Chem. Lett.* **2017**, *8*, 5523–5530.
- (54) Sakthivel, N. A.; Theivendran, S.; Ganeshraj, V.; Oliver, A. G.; Dass, A. Crystal Structure of Faradaurate-279: Au₂₇₉(SPh-tBu)₈₄ Plasmonic Nanocrystal Molecules. *J. Am. Chem. Soc.* **2017**, *139*, 15450–15459.
- (55) Joshi, C. P.; Bootharaju, M. S.; Alhilaly, M. J.; Bakr, O. M. $[Ag_{25}(SR)_{18}]^-$: The "Golden" Silver Nanoparticle. *J. Am. Chem. Soc.* **2015**, *137*, 11578–11581.
- (56) Taylor, M. G.; Mpourmpakis, G. Rethinking Heterometal Doping in Ligand-Protected Metal Nanoclusters. *J. Phys. Chem. Lett.* **2018**, *9*, 6773–6778.
- (57) Zhao, J.; Jin, R. Heterogeneous catalysis by gold and gold-based bimetal nanoclusters. *Nano Today* **2018**, *18*, 86–102.